



Trends and Spatio-Temporal Variability of Summer Mean and Extreme Precipitation across South Korea for 1973–2022

Hye-Ryeom Kim^{1,2} · Mincheol Moon^{3,4} · Junghee Yun^{2,4} · Kyung-Ja Ha^{1,2,3,4}

Received: 21 December 2022 / Revised: 5 March 2023 / Accepted: 21 March 2023 / Published online: 6 April 2023
© The Author(s) under exclusive licence to Korean Meteorological Society and Springer Nature B.V. 2023

Abstract

Climate change has altered the frequency, intensity, and timing of mean and extreme precipitation. Extreme precipitation has caused tremendous socio-economic losses, and severe impacts on human life, livelihood, and ecosystems. In recent years, heavy rainfall events occurred during the boreal summer (June-to-August) frequently and sporadically over South Korea. Given that its severity, a call for an urgent investigation of summer extreme rainfall is needed. Although many previous studies have addressed daily extreme precipitation, hourly extreme rainfall still needs to be thoroughly investigated. Therefore, in this study, we investigated the trends, spatio-temporal variability, and long-term variations in mean and extreme precipitation over South Korea during the boreal summertime using daily and hourly observational data through various analysis methods. During the past 50 years (1973–2022), there has been a notable escalation in maximum hourly precipitation, although the boreal summer mean precipitation has increased only marginally. Regionally, an increase in mean and extreme rainfall occurred in the northern part of the central region and the southern coast of the Korean peninsula. Moreover, the increase in intensity and frequency of extreme precipitation as well as in dry day have contributed more to the total summer precipitation in recent years. Our findings provide scientific insights into the progression of extreme summer precipitation events in South Korea.

Keywords Extreme precipitation · Climate change · Spatio-temporal variability · Hourly-maximum precipitation · Long-term variations · Automated Surface Observing System (ASOS)

1 Introduction

Climate change has a significant impact on the Earth system. Globally, total human-induced surface air temperature increased by approximately 1.07 °C (0.8 °C to 1.3 °C) from 1850 to 2019 (IPCC 2022). In tandem with rising temperatures, worldwide mean precipitation tends to increase in response to an increased water-holding capacity of the

atmosphere (Allen and Ingram 2002; Held and Soden 2006). On a physical basis, the atmospheric moisture-holding capacity will increase exponentially at a rate of about 6 to 7% per degree of warming based on the Clausius-Clapeyron (C–C) relation (Trenberth et al. 2003). Thus, extreme rainfall is expected to intensify in response to anthropogenic warming (Allan and Soden 2008; O’Gorman and Schneider 2009; Craig 2010; Oh et al. 2018). The frequency and intensity of heavy rainfall have increased considerably since 1951 while light precipitation has decreased in frequency, and it varies strongly between regions and subregions (Trenberth et al. 2003; Alexander et al. 2006; Kharin et al. 2007; Min et al. 2011; Chou et al. 2012; Ha et al. 2020a; IPCC 2022). The Intergovernmental Panel on Climate Change (IPCC) also pointed out that climate change could affect the frequency, intensity, and timing of extreme events such as heatwaves, droughts, tropical cyclones, and extreme rainfall events (IPCC 2022). As one of the most hazardous extreme phenomena, extreme rainfall events bring considerable damage to human life, ecosystems, and the social economy of agriculture, resulting in secondary disasters including landslides

Communicated by Jong-Seong Kug.

✉ Kyung-Ja Ha
kjha@pusan.ac.kr

¹ BK21 School of Earth and Environmental Systems, Pusan National University, Busan, Republic of Korea

² Department of Atmospheric Sciences, Pusan National University, Busan, Republic of Korea

³ Department of Climate System, Pusan National University, Busan, Republic of Korea

⁴ Center for Climate Physics, Institute for Basic Science, Busan, Republic of Korea

and flash floods by causing colossal socioeconomic losses (Dave et al. 2021; Kim et al. 2021; Meyer et al. 2021; Ning et al. 2021). Therefore, it is essential to understand extreme rainfall events.

Compared to the global mean surface warming, South Korea has experienced considerably greater surface warming because of the complex influence of several climate variabilities along the northeastern coast of Asia (Jung et al. 2002; An et al. 2011). In terms of linear trends, the local temperatures have risen by 1.90 °C (1912–2014), 1.35 °C (1954–2014), and 0.99 °C (1973–2014), which are 1.4–2.6 times greater than the global land mean temperature increases (Park et al. 2017). Regarding global warming, particularly for the Korean Peninsula (KP), a growing number of previous studies proposed that the frequency and intensity of extreme weather events (i.e., extreme precipitation events, droughts, heat waves, and tropical cyclones) have increased over the past few decades (Kim et al. 2012; Lee et al. 2012; Min et al. 2015; Ha et al. 2020b; Park et al. 2021; Seo et al. 2021). Especially, for extreme precipitation, Korea is greatly influenced by the East Asian summer monsoon. As one of the primary factors of heavy rainfall events, the Changma and typhoons greatly impact extreme precipitation. The Changma, as a part of the East Asian summer monsoon, is most active between early July and early September, with the first Changma starting in late June and ending in late July (Seo et al. 2011; Park et al. 2015; Lee et al. 2017). Following Preethi et al. (2017), the summer monsoon precipitation over South Korea has displayed an increasing trend in the recent few decades. On the other hand, the second Changma is mainly associated with typhoons in late summer, and typhoons intensively affect the KP in July, August, and September (Lee et al. 2017; Moon and Ha 2021). Heavy rainfall in the KP during the boreal summer needs to be investigated because the sub-seasonal variability is very large, even during summer.

Specifically, in 2020, unprecedented heavy rains during the summer occurred due to a considerable reduction in aerosol layers by initiating the COVID-19 lockdown (Kripalani et al. 2022). In addition, these consecutive heavy rainfalls led to severe floods and induced 46 casualties as well as billion-dollar economic losses (KMA 2021). Also, this summer, the metropolitan area endured particularly heavy torrential rain and flooding. In Seoul, an hourly downpour of 141.5 mm/hr was recorded, which was the heaviest hourly precipitation breaking the record in 80 years (Bae and Yeung 2022). This event surpassed 381.5 mm, which was the heaviest daily precipitation recorded in the past 102 years. At least 14 people died because of heavy rainfall, and the total sum of the damage was estimated to exceed 50 million-dollar. Several studies have investigated the changes in mean and extreme rainfall in South Korea (Ho et al. 2003; Jung et al. 2011; Baek et al. 2017; Azam et al. 2018). Most of

these studies focused on daily extreme precipitation, therefore, our understanding of hourly extreme rainfall events is insufficient. However, hourly extreme precipitation should be highlighted because it can induce great damage, as we have already experienced.

On the other hand, it is necessary to understand long-term variations and trends in mean and extreme precipitation in water resource and flood risk management (Moberg et al. 2006; Ha et al. 2009; Pei et al. 2017; Kim and Ha 2021; Wang et al. 2021; Hu et al. 2022; Ryan et al. 2022). The ensemble empirical mode decomposition (EEMD) method is employed to appropriately reflect nonlinear responses to global warming and urbanization (Yun et al. 2018; Jeong et al. 2022). Kim et al. (2018) revealed that through the EEMD analysis, the long-term variation of monthly precipitation in South Korea was strongly correlated with the Atlantic Multi-decadal Oscillation (AMO).

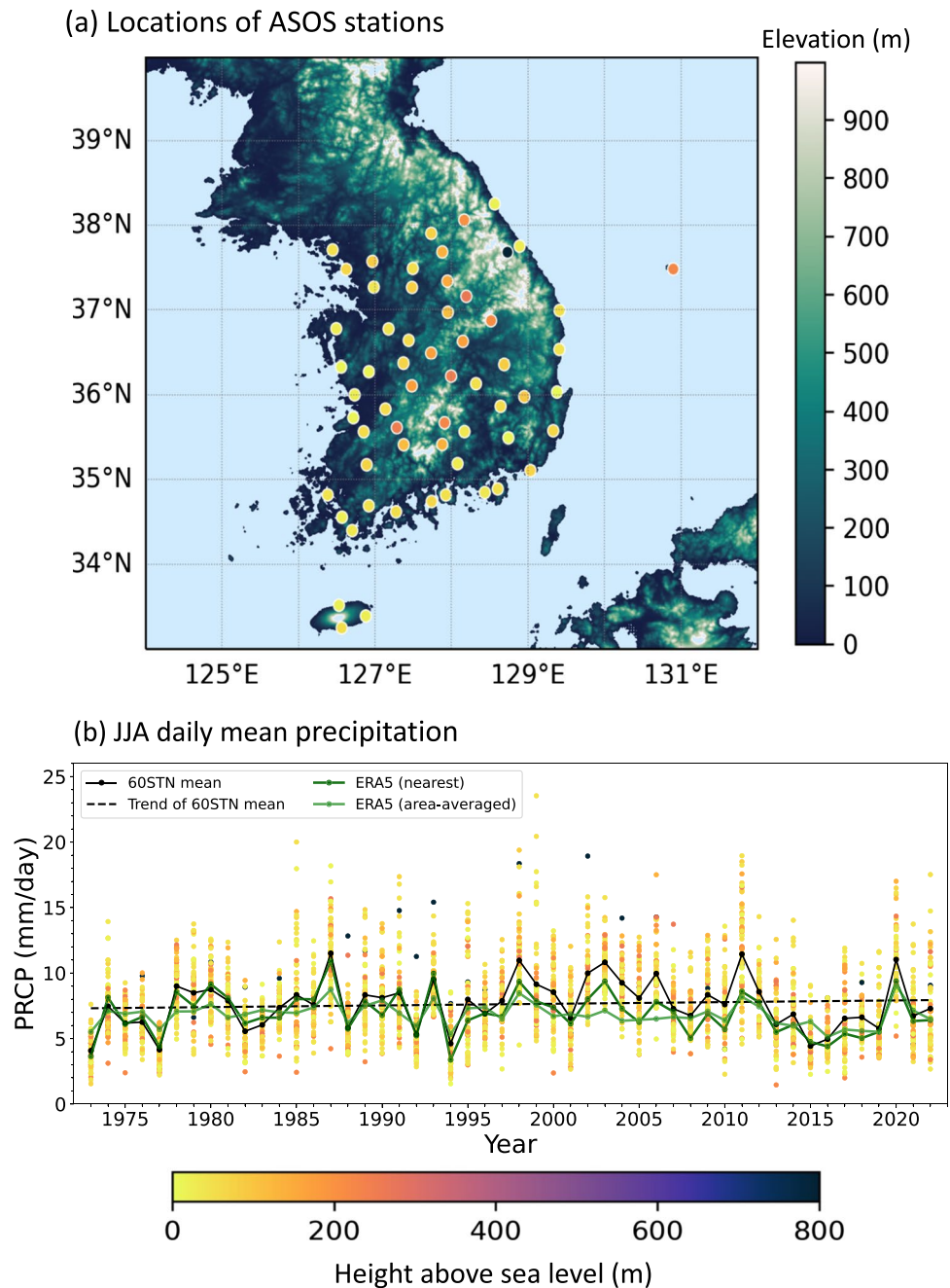
Consequently, the purpose of this study was as follows: (1) to analyze the trends of extreme precipitation in terms of hourly and daily time scales, as well as their spatial patterns over South Korea; (2) to focus on long-term variations in the mean temperature and extreme precipitation by applying the EEMD method; and (3) to identify the recent changes in major spatio-temporal distributions of summertime precipitation.

2 Data and Methods

2.1 Data

We used daily mean precipitation, 1-h maximum precipitation, and daily mean temperature from the Automated Surface Observing System (ASOS) for the investigation of trends and variability in Korean summer rainfall from 1973 to 2022. Sixty stations out of a total of 103 stations were selected, encompassing the entire analysis period (Fig. 1a). The months of June–July–August (JJA) are regarded as the boreal summer. Hourly precipitation data were obtained from the European Center for Medium-Range Weather Forecasts reanalysis version 5 (ERA5; Hersbach et al. 2020). We adjusted the time in line with Korea Standard Time (KST) owing to the time difference between the Universal Time Coordinate (UTC) and KST. For the ERA5 reanalysis data, the area-averaged precipitation over South Korea and the nearest grid point precipitation were compared to the ASOS total station mean precipitation. The Pearson Correlation Coefficient (PCC) was calculated to examine the relations between each way of ERA5 (the area-averaged and the nearest grid point) and observations. The area-averaged (the nearest grid point) precipitation and observations have a PCC of 0.75 (0.89), statistically significant above the 99% confidence level (p -value < 0.01).

Fig. 1 (a) Topographical sketch map of South Korea with 60 ASOS stations (circles, bottom colored bar). The shading displays the topographic elevation (upper-right colored bar). (b) Interannual variability in summertime (JJA) daily precipitation at each station over the past 50 years (1973–2022). The solid black line represents the JJA mean precipitation of all stations, and its trend is indicated via a black dashed line. For the ERA5 dataset, the nearest grid point of each station (solid dark olive-green line) and area-averaged value (solid yellow-green line) are also exhibited



In addition, the Root Mean Squared Error (RMSE) was implied to evaluate the accuracy of the reanalysis data. The area-averaged and the nearest grid precipitation showed the RMSE with the value of 1.56 and 1.12, respectively. Instead of area-averaged precipitation, the nearest grid point precipitation corresponded more closely with the ASOS. However, since the late 1990s, the ERA5 dataset has tended to underestimate the JJA mean precipitation from the ASOS (Fig. 1b). In particular, when the JJA mean precipitation

was at its peak, ERA5 data could not match the observation. A heavy rainfall event is typically a localized event occurring in a small area. Therefore, ERA5, which had a spatial resolution of approximately 30 km, was not sufficient to simulate these peak events in observation. This was consistent with that of Borodina et al. (2017) and highlighted the importance of observational data in studying localized heavy rainfall events. In terms of the topography, the ETOPO1 dataset was selected (Amante and Eakins 2009).

2.2 Extreme Indices

Five indices derived from the Expert Group on Climate Change Detection and Indices (ETCCDI) were calculated to describe the features of extreme precipitation (Table 1). A wet day indicated that the daily precipitation amount was more than 1 mm (Yao et al. 2008; Kim et al. 2013). The total precipitation (PRCPTOT) was the sum of precipitation on wet days. Extremely wet day total precipitation denoted instances where the daily precipitation exceeded the 95th and 99th percentiles of the wet day precipitation (R95p, R99p); this was calculated during the summer. In addition, the ratio of JJA precipitation to annual precipitation and the hourly maximum precipitation displayed a significant decadal change in the 1990s and the early 2000s (Fig. 1). Thus, to compare the changes in summertime precipitation, we divided the 50 years into two periods: 1973–1992 (P1, reference period) and 2003–2022 (P2), and calculated each percentile value for the reference period. For frequency, we used the number of heavy precipitation days when the daily precipitation amount was more than 20 mm (R20mm) and the number of dry days when the daily precipitation was less than 1 mm. We defined the number of days with R95p and R99p as R95pF and R99pF, respectively. The hourly extreme precipitation index (RX1H) was defined as the maximum 1-h precipitation; this index was used to focus on heavy downpours in a short period. Many studies have assessed the effect of urbanization on temperature and precipitation trends in South Korea (Ha et al. 2004; Park et al. 2017). In Sect. 3.3, we selected a high-population group with a population of more than 1,000,000 and a low-population group with a population of less than 50,000 in order to examine the effects of urbanization on extreme precipitation (Table 2).

Table 1 Definitions of precipitation extreme indices

Indices	Definition	Unit
PRCPTOT	Total precipitation from days with PRCP ≥ 1 mm	mm
RX1H	Maximum 1-h precipitation	mm
R95p	Total precipitation when PRCP ≥ 95 th percentile	mm
R99p	Total precipitation when PRCP ≥ 99 th percentile	mm
R95pF	Number of days when PRCP ≥ 95 th percentile	days
R99pF	Number of days when PRCP ≥ 99 th percentile	days
R20mm	Number of days with PRCP ≥ 20 mm	days
Dry day	Total precipitation from days with PRCP < 1 mm	days

2.3 Ensemble Empirical Model Decomposition (EEMD)

Ensemble Empirical Mode Decomposition (EEMD) is an improved noise-assisted data analysis method, developed

to solve the problem of mode mixing in Empirical Mode Decomposition (EMD). The EEMD decomposes the original signals ($x(t)$) into a finite number (N) of independent signals with periodicity ($C_i(t), i = 1, 2, 3, \dots, n$) and a residual linear or nonlinear trend ($R(t)$) (Wu and Huang 2004, 2009).

$$x(t) = \sum_{i=1}^n C_i(t) + R(t) \tag{1}$$

The EEMD procedure is as follows. First, add the white noise time series ($w(t)$) having a normal or gaussian distribution to the original time series ($x(t)$). At this time, the added noise has an amplitude of α .

$$x_1(t) = x(t) + \alpha w_1(t) \tag{2}$$

Second, find the local maxima and minima of the time series ($x_1(t)$) and create the upper and lower envelopes ($x_{u1}(t)$ and $x_{l1}(t)$) by connecting local maxima and minima using cubic spline interpolation. Third, calculate the mean of the upper and lower envelopes ($m_{1,1}(t) = (x_{u1}(t) + x_{l1}(t)) / 2$) and subtract the mean ($m_{1,1}(t)$) from the $x_1(t)$.

$$h_{1,1} = x_1(t) - m_{1,1}(t) \tag{3}$$

Fourth, repeat steps 2 and 3 k times until $m_{1,k}(t) = 0$.

$$\begin{aligned} h_{1,2} &= h_{1,1}(t) - m_{1,2}(t) \\ &\dots \\ h_{1,k} &= h_{1,k-1}(t) - m_{1,k}(t) \end{aligned}$$

When $m_{1,k}(t) = 0$, $h_{1,k}$ is regarded as $C_{1,1}$. Fifth, subtract $C_{1,1}$ from $y_1(t)$.

$$r_{1,1}(t) = x_1(t) - C_{1,1}(t) \tag{4}$$

Sixth, replace $x_1(t)$ with $r_{1,1}(t)$ in step 2 and go through steps 2–5. Through this process, $C_{2,1}(t)$ is obtained. As step 6 is repeated, n periodic components of the first sequence ($C_{n,1}(t)$) are produced, and finally, the residual trend ($r_{n,1}(t)$) is left. Seventh, generate the white-noise time series again in step 1.

$$x_2(t) = x(t) + \alpha w_2(t) \tag{5}$$

And repeat steps 1–6 m times. After m iterations, calculate the ensemble mean of each periodic component. The ensemble mean removes the white noise signals added in step 1.

$$C_i(t) = \frac{1}{m} \sum_{j=1}^m C_{i,j}(t), i = 1, 2, \dots, n. \tag{6}$$

Here, the standard deviation of the added noise series (α) and the ensemble number (m) for EEMD were entered as 0.2 and 200, respectively.

Table 2 Information for high- and low-population stations (latitude, longitude, above sea level height, population)

	Station	Latitude (°)	Longitude (°)	Above sea level Height (m)	Population
High-population	Seoul	37.57	126.97	85.50	9,682,126
	Busan	35.10	129.03	69.56	3,370,450
	Incheon	37.48	126.62	68.15	2,948,375
	Daegu	35.83	128.65	53.40	2,412,642
	Daejeon	36.37	127.37	70.22	1,446,863
	Gwangju	35.17	126.89	72.38	1,432,049
	Suwon	37.27	126.99	34.84	1,216,965
	Ulsan	35.56	129.32	34.57	1,132,713
Low-population	Uljin	36.99	129.41	50.00	47,858
	Wando	34.40	126.70	35.24	49,458
	Hapcheon	35.57	128.17	32.00	42,181
	Namhae	34.82	127.93	45.71	42,266
	Jangheung	34.69	126.92	45.02	36,622
	Yeongdeok	36.53	129.41	41.20	35,314
	Sancheong	35.41	127.88	138.07	34,360
	Boeun	36.49	127.73	171.31	31,587
	Inje	38.06	128.17	201.78	32,192
	Imsil	35.61	127.29	247.04	27,003
	Ulleungdo	37.48	130.90	222.80	8,888

2.4 Extended Empirical Orthogonal Function (EEOF)

The Extended Empirical Orthogonal Function Analysis (EEOF) was employed in conjunction with reanalysis data to analyze the temporal evolution of the principal spatial structure. The traditional EOF is that the variable divided to spatial and temporal mode. The eigenvector and eigenfunction for an atmospheric variable, μ_{ij} , were as follows:

$$\mu_{ij} = \sum_{l=1}^{l=L} \alpha_{il} \Psi_{jl} \quad (7)$$

where i indicates the space, j denotes the time, l is the mode number, α_{il} is the space structure of eigenfunction, and Ψ_{jl} is a function of temporal variation.

However, the spatial field has temporal autocorrelation, and to account for this, to analyze the evolution of dominant modes at specific temporal lags through EEOF. Several previous studies have applied EEOF to investigate the evolution of the substructure (Chen and Harr 1993; Kim et al. 2008). Using the EEOF analysis, we interpreted the substructure as the propagation or evolution of the sub-seasonal mode over time of the first substructure of the function. The eigenvector and eigenfunction for an atmospheric variable of sub-structure, $\mu_{ij}^{(n)}$, were as follows:

$$\alpha_{il}^{(n)} = \sum_{j'=1}^{j'=J'} \mu_{ij'}^{(n)} \Psi_{j'l} \quad (8)$$

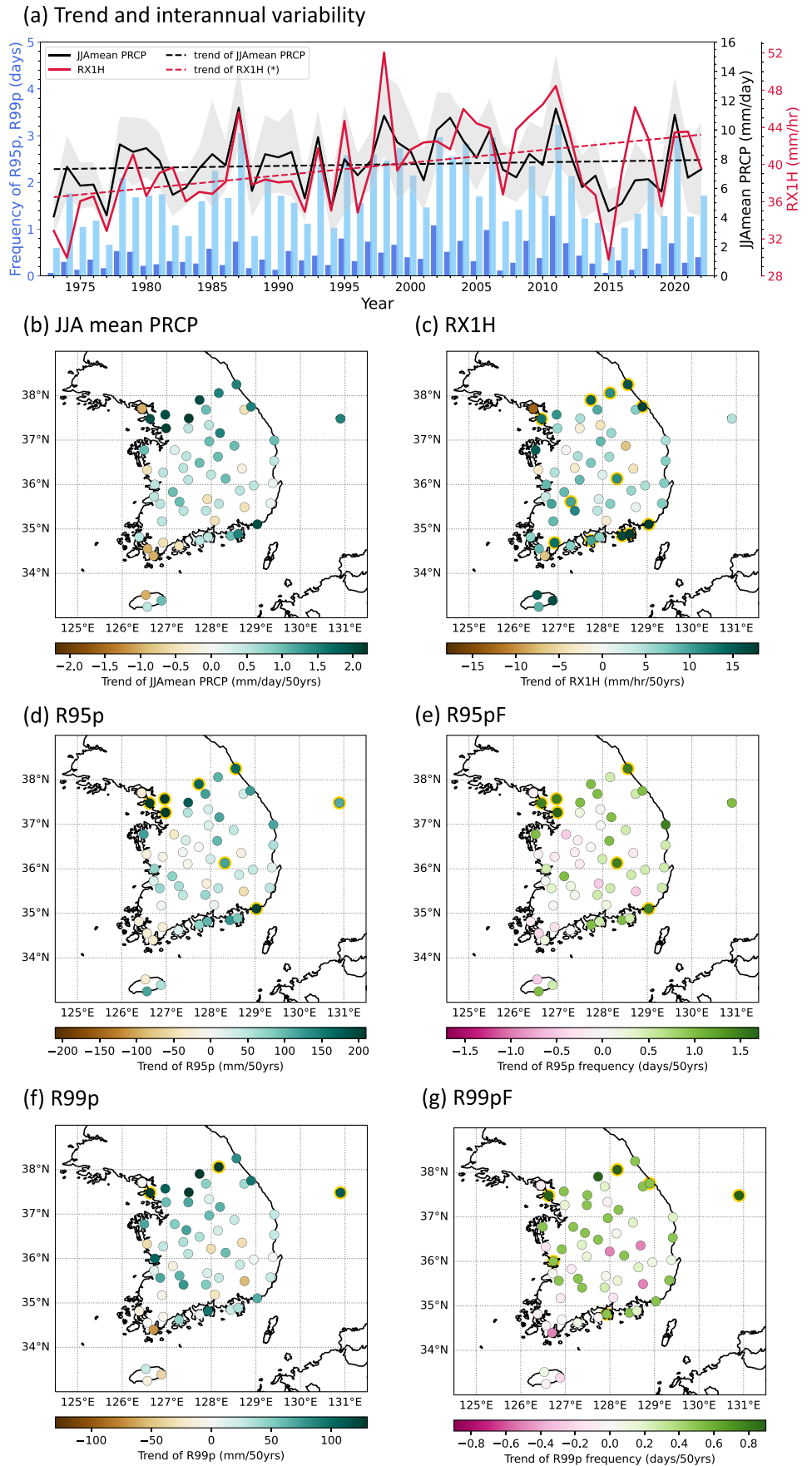
where j' indicates time in the window, and n represents the number of windows. $\Psi_{j'l}$ is a function of temporal variation in the window, and $\alpha_{il}^{(n)}$ is n -th window-averaged space structure with the l -th eigenfunction serving as the weight. In a previous study, a window size of 20 days was used to focus on quasi-stationary properties (Kim et al. 2008). In this study, we set the window size (substructure) as the minimum sub-seasonal time scale (2 weeks) with a lag of 6 days to analyze the evolution of precipitation in the finer sub-seasonal mode. The number of windows (n in Eq. (2)) was 14, from June 1 to August 31.

3 Results

3.1 Boreal Summer Mean and Extreme Precipitation from 1973 to 2022

To determine the interannual variability (IAV) of the JJA mean daily precipitation, we calculated the IAV for each station between 1973 and 2022. Figure 1b depicts the IAV of each ASOS station, the total stations mean, and area-averaged precipitation over South Korea as well as the closest grid point values of ERA5. The IAV of the JJA mean precipitation shows large differences among stations. Similarly, in Fig. 2a (grey shading), the JJA mean precipitation exhibits a large deviation among ASOS stations. Additionally, it shows great spatial variability, especially

Fig. 2 (a) Time series of boreal summer daily mean precipitation (JJA mean precipitation, solid black line) with its trend (dashed black line) and spatial variability (grey shading) from 1973 to 2022. Extreme indices, hourly-maximum precipitation (RX1H, solid red line) and its trend (dashed red line), as well as the frequencies of R95p (R95pF, light sky-blue bar) and R99p (R99pF, blue bar). The spatial patterns of the trends over the past 50 years are presented in (b) JJA mean precipitation (mm/day/ 50yrs), (c) RX1H (mm/hr/50 yrs), (d) R95p (mm/50 yrs), (e) R95pF (days/50 yrs), (f) R99p (mm/50 yrs), (g) R99pF (days/50 yrs). The enclosed yellow indicates statistical significance at a 90% confidence level



in the northern part of the central region and the south coast of the KP, and Jeju island (Fig. R2). This result supported the notion that precipitation in South Korea displayed strong spatial variability (Jung et al. 2011). In addition, the station mean of JJA mean precipitation exhibited a slightly increasing trend of 0.65 mm/day over 50-year period, but it was not statistically significant. Spatially, 80% of the total stations (48 of 60 stations) presented an increasing trend in JJA mean precipitation, whereas 20% displayed a decreasing trend, which was not significant (Fig. 2b). Specifically, 20% of total stations (12 of 60 stations) showed a greater increasing trend (above 1.5 mm/day) over the 50 years, and most of these stations were concentrated in the northern part of the central region near 38°N and some southern coastal regions such as Geoje and Busan (Table S1).

Five indices were calculated as indicators of extreme precipitation: RX1H, R95p, R99p, R95pF, and R99pF. These indices showed an increasing trend for the 50 years, but only two had significant increasing trends at a 90% significance level (Table 3). Figure 2a displays the IAV and trends for the extreme indices from 1973 to 2022. While JJA mean precipitation showed a very slight increase (0.65 mm/day/50 yrs), RX1H presented a very clear increasing trend (7 mm/hr/50 yrs) at a 99% significance level (Table 3). The linear trends of R95p (R99p) and R95pF (R99pF) were 60.5 mm/50 yrs (37 mm/50 yrs) and 0.5 days/50 yrs (0.2 days/50 yrs) for the same period, respectively. Figure 2c–g show the spatial distribution of the linear trend for each extreme precipitation index. For RX1H, 50 (10) stations, which accounted for 83.3% (16.7%) of the total stations, showed an increasing (decreasing) trend over the past five decades. Twelve stations (20%) had a significant increasing trend for RX1H (Fig. 2c). Most of the significant stations were concentrated in the northern portion of the central region, along with the southern coast of Korea. Additionally, some stations, such as Imsil and Gumi, were located on inland regions. For R95p, 47 (13) stations, which equate to 78.3%

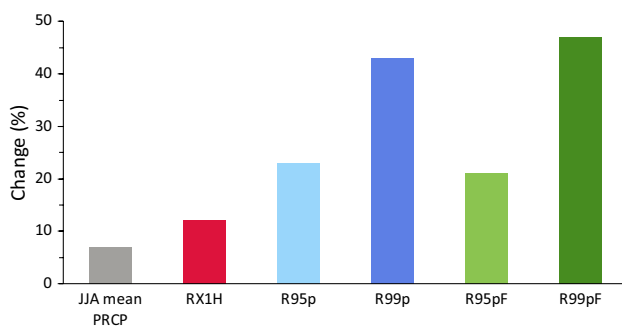


Fig. 3 Observed changes (%) in the mean and extreme precipitation over South Korea between P1 (1973–1992) and P2 (2003–2022)

Table 3 The trend of precipitation indices for all ASOS stations mean over the past 50 years (1973–2022). The star (*) indicates statistical significance above a 90% confidence level

Station	JJA mean PRCP (mm/day)	RX1H (mm/hr)	R95p (mm)	R99p (mm)	R95pF (days)	R99pF (days)
60STN mean	0.65	7.00 *	60.50	37.00	0.50	0.20 *

(21.7%), showed increasing (decreasing) trends, and seven stations (approximately 13%) showed significant increasing trends (Fig. 2d). The frequency of R95p occurred more (less) frequently at 43 (17) stations, comprising 71.7% (28.3%) of total stations. Specifically, six stations (10%) displayed increasing trends in R95pF, and their locations were identical to those of R95p, except for one less station (Fig. 2e). An increasing (decreasing) trend for R99p was observed at 46 (14) stations, comprising 76.7% (23.3%) of total stations. Specifically, only 3 (5%) stations, namely Incheon, Inje, and Ulleungdo Island, exhibited a significant increasing trend (Fig. 2f). Likewise, the frequency of R99p tended to increase (decrease) at 45 (15) stations, with 75% (25%) and six stations (10%) experiencing significant increases. These stations are primarily located in the northern and several coastal regions (Fig. 2g). In general, extreme precipitation intensified in the northern portion of the South and certain coastal regions. The exception was the inland basin of Gumi, which also experienced significant increases in RX1H, R95p, and R95pF.

The changes in JJA mean rainfall and each extreme precipitation index between the P1 and P2 revealed the evolution of daily precipitation in South Korea over the past two decades (Fig. 3). The increase in the JJA mean precipitation rate was 6.71%. Given that the JJA mean precipitation was 7.63 mm/day for 50-year period, higher summer precipitation was indicated in P2 with a value of 7.72 mm/day, whereas 7.24 mm/day was depicted in P1. The RX1H increased by 12.28%. In addition, R95p (R95pF) tended to increase by approximately 22.85% (20.91%). A notable increase in R99p (R99pF) was observed, at a rate of 43.23% (47.3%), during P2. In addition, South Korea exhibited salient intraseasonal variability; therefore, there was a need to divide the summer season into monthly segments (Ha and Oh 2019; Jia et al. 2022; Ren et al. 2022). The monthly average precipitation was the highest in July (8.99 mm/day), followed by August (8.55 mm/day), and June (5.26 mm/day) (Table 4). In P1 and P2, monthly mean precipitation increased in July (P1: 8.63 mm/day, P2: 9.92 mm/day) and August (P1: 7.58 mm/day, P2: 8.46 mm/day), whereas it decreased in June (P1: 5.44 mm/day, P2: 4.68 mm/day)

Table 4 Monthly mean precipitation during the boreal summer for the whole period, P1, and P2

	Monthly mean PRCP (mm/day)		
	Whole Period	P1 (1973–1992)	P2 (2003–2022)
June	5.26	5.44	4.68
July	8.99	8.63	9.92
Aug	8.55	7.58	8.46

(Table 4). R95p (R95pF) and R99p (R99pF) comprised the largest portions at 40.93% (41.12%) and 42.76% (43.16%) in July, respectively, which was followed by August at 38.04% (34.74%) and 39.15% (35.71%), as well as June at 21.03% (24.14%) and 18.09% (21.13%), respectively, for 1973–2022 (Table 5). The amount and frequency of extreme precipitation were mostly concentrated in July. Comparing P1 and P2, this trend became more pronounced in P2. For P1, R95p (R95pF) was 25.17% (27.52%), 38.21% (38.87%), and 36.62% (33.62%) in June, July, and August, respectively. Similarly, R99p (R99pF) constituted 24.37% (27.52%), 39.31% (39.37%), and 36.32% (33.11%) in June, July, and August, respectively (Table 5). During P2, R95p (R95pF) accounted for 17.05% (19.81%), 49.78% (49.00%), and 33.17% (31.19%) in June, July, and August, respectively. In the case of R99p (R99pF), 15.27% (18.13%), 54.41% (53.51%), and 30.32% (28.36%) were observed in June, July, and August, respectively (Table 5). In P2, extreme

precipitation decreased in June, except for R99pF. Although these four indices increased in July and August, a much further increase was observed in July. Thus, the ratio of extreme indices appeared to decline in August in P2, whereas there was an increase in extreme rainfall occurs in July.

3.2 Long-term Variations in Mean Temperature and Extreme Precipitation Indices

The EEMD decomposed the mean temperature (TEMP) and extreme precipitation indices (PRCPTOT, RX1H, R95p, R20mm, and Dry day) into four interannual to interdecadal components (C1 to C4) and one residual trend (Table 6). For 1973–2022, C1 and C2 of all indices showed approximately 2.7- to 2.9-year and 5.4- to 5.7-year periodic oscillations, accounting for approximately 51.8 to 60.1% and 18.3 to 22.5% of the total variance, respectively. C3 and C4 show approximately 10.6- to 11.7-year and 24.6- to 30.4-year oscillations and contribute about 8.4 to 10.9% and 3.4 to 5.4% of the total variance, respectively. The residual trend was 7.0 to 15.9%. Compared with other extreme precipitation indices, TEMP has a high variance of the residual trend by 6 to 9%. To shed light on the long-term changes in the mean temperature and extreme precipitation indices, we defined long-term variations as the sum of decomposed components with more than 10 years of mean periods (C3 and C4) and residuals. The linear

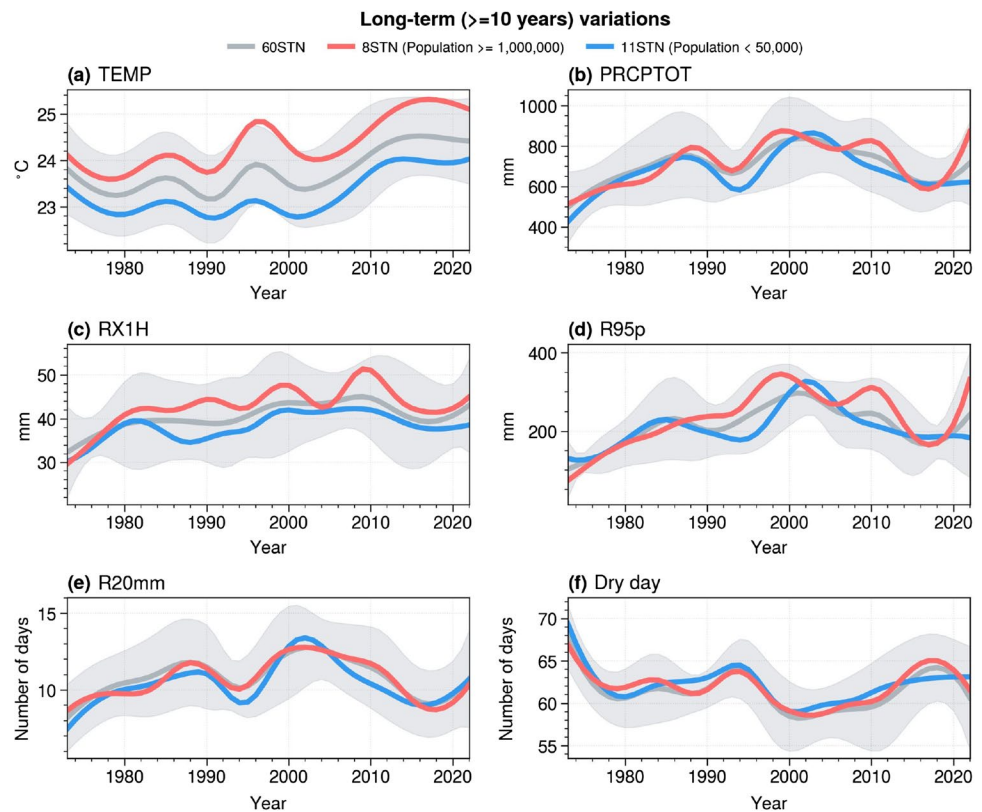
Table 5 Portions of each month during the boreal summer for each variable

	R95p (%)			R99p (%)			R95pF (%)			R99pF (%)		
	Whole Period	P1	P2	Whole Period	P1	P2	Whole Period	P1	P2	Whole Period	P1	P2
June	21.03	25.17	17.05	18.09	24.37	15.27	24.14	27.52	19.81	21.13	27.52	18.13
July	40.93	38.21	49.78	42.76	39.31	54.41	41.12	38.87	49.00	43.16	39.37	53.51
Aug	38.04	36.62	33.17	39.15	36.32	30.32	34.74	33.62	31.19	35.71	33.11	28.36

Table 6 Mean periods (year) and their variance contribution (%) of mean temperature (TEMP), PRCPTOT, RX1H, R95p, R20mm, and Dry day at 60 stations

		C1	C2	C3	C4	R
TEMP	Mean Period (year)	2.9	5.7	11.7	30.3	
	Variance (%)	51.8	18.3	10.2	3.8	15.9
PRCPTOT	Mean Period (year)	2.7	5.7	11.5	30.4	
	Variance (%)	54.4	22.5	9.9	3.4	9.8
RX1H	Mean Period (year)	2.8	5.7	10.9	29.4	
	Variance (%)	55.7	21.0	10.9	4.9	7.5
R95p	Mean Period (year)	2.7	5.4	10.6	28.7	
	Variance (%)	56.8	19.9	10.9	5.4	7.0
R20mm	Mean Period (year)	2.7	5.6	11.4	28.7	
	Variance (%)	56.6	22.5	9.8	3.6	7.5
Dry day	Mean Period (year)	2.8	5.6	11.2	24.6	
	Variance (%)	60.1	20.2	8.4	4.3	7.0

Fig. 4 Long-term variations of (a) mean temperature ($^{\circ}\text{C}$), (b) PRCPTOT (mm), (c) RX1H (mm), (d) R95p (mm), (e) R20mm (days), and (f) dry day (days) from 1973 to 2022 at 60 stations (grey line); 8 stations had a population of 1 million or more (red line), and 11 stations with a population of 50,000 or less (blue line). Grey-shaded areas represent one standard error of the mean values from 60 stations. Long-term variations were defined as the sum of decomposed components with mean periods and residuals exceeding 10 years. 8STN (population $\geq 1,000,000$): Seoul, Busan, Incheon, Daegu, Daejeon, Gwangju, Suwon, and Ulsan. 11STN (population $< 50,000$): Uljin, Wando, Hapcheon, Namhae, Jangheung, Yeongdeok, Sancheong, Boeun, Inje, Imsil, Ulleungdo

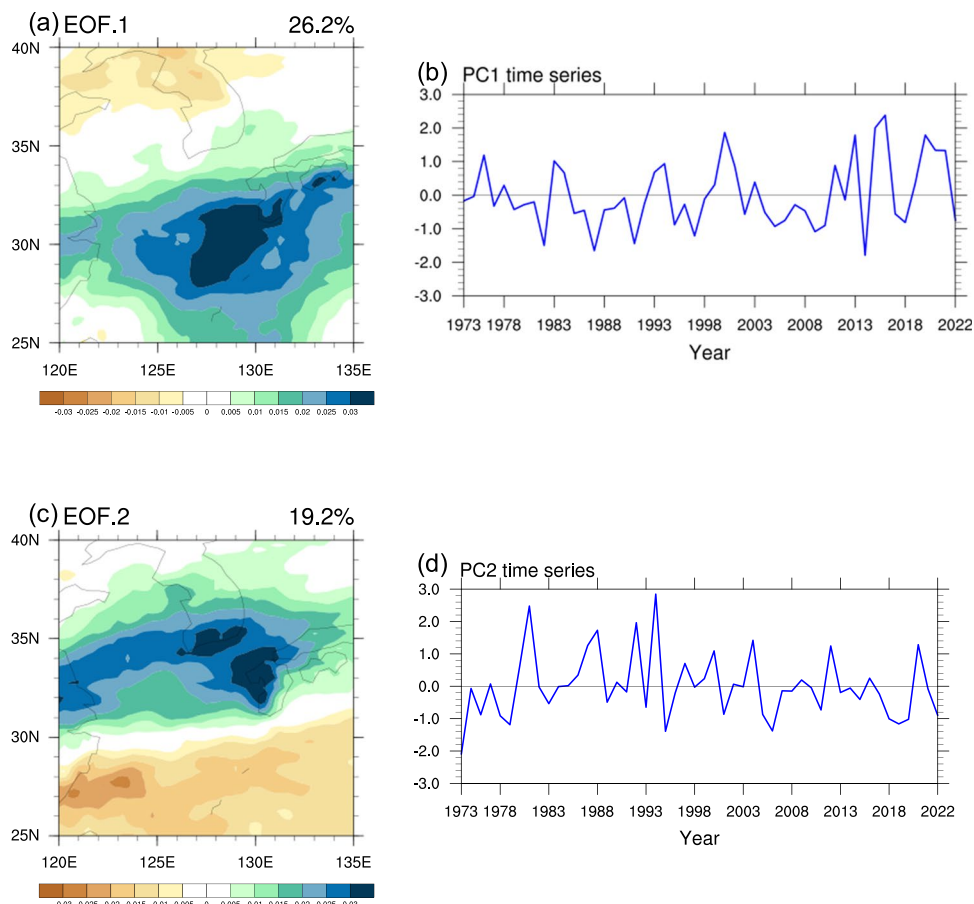


trends in mean temperatures in high-population regions ($0.03\text{ }^{\circ}\text{C}/\text{year}$) were faster than those in low-population regions ($0.02\text{ }^{\circ}\text{C}/\text{year}$) (Fig. 4a). This result corresponds to the fact that big cities have experienced greater warming because of rapid urbanization and population growth since 1973 (KMA 2021). On the one hand, the long-term variations decomposed through EEMD showed that long-term changes in mean temperature and PRCPTOT did not occur simultaneously. The mean temperature increased, with multi-decadal fluctuations entering a phase higher than the mean temperature ($23.7\text{ }^{\circ}\text{C}$) from the mid-2000s and stabilizing at 24.4 to $24.5\text{ }^{\circ}\text{C}$ after 2010 (Fig. 4a). However, PRCPTOT was in a phase higher than the mean PRCPTOT (698.7 mm) from the mid-1990s to 2010. It peaked at 837 mm in 2002 and decreased to 613.7 mm in 2017. Since then, it has soared (Fig. 4b). RX1H, R95p, and R20mm also displayed similar features to PRCPTOT (Fig. 4c-e), and the dry day was negatively correlated with PRCPTOT, with a correlation coefficient of -0.857 ($p\text{-value} < 0.01$) (Fig. 4f), indicating that the frequency and intensity of extreme precipitation contributed significantly to PRCPTOT and implying that the increase in the number of dry days and the increase in the frequency and intensity of extreme precipitation during the recent years have greatly influenced the total precipitation in summer.

3.3 Sub-seasonal Modes of Precipitation across East Asia during the Boreal Summer

Prior to understanding the sub-seasonal mode, we applied empirical orthogonal function (EOF) analysis to the JJA (June–July–August) daily rainfall averaged over East Asia (EA) [120°E – 135°E , 25°N – 40°N] from 1973 to 2022 to extract the dominant modes of interannual variability in precipitation (Fig. 5). The pattern of a precipitation band formed near 30°N appeared as the dominant mode 1, explaining 26.2% of the summer variability (Fig. 5a), while the pattern of the precipitation band moving northward and affecting the Korean Peninsula and Fukuoka area was shown to explain 19.2% (Fig. 5b). Looking at the PC time series, the intensity variation of the PC after the 2000s changes more significantly than that of the 1970s–1990s. To investigate this major difference in interannual variability, we divided the dataset into the early 20 years (1973–1992; hereafter P1) and the later 20 years (2003–2022; hereafter P2) for analysis. Since it is difficult to explain the temporal evolution of the sub-seasonal mode using the existing EOF, we analyzed the 20-year averaged daily precipitation in the EA for P1 and P2 using the EEOF. The first mode of EEOF accounted for about 84.9% of the total variance and clearly demonstrated the

Fig. 5 The pattern correlation (red line) between P1 and P2. Difference between maximum location and minimum location is displayed with bar for each window



spatio-temporal evolution of daily precipitation throughout EA (Fig. 6).

The stationary precipitation core in the Satsunan Islands, which appeared in the first window (6/1–6/14) near 30°N, developed over time and moved to the KP in the eighth window (7/13–7/26). The spatial distribution of precipitation revealed a core in the north KP and a weak signal in the south KP from the ninth window (mid-July) to the 11th window (early August). In addition to the precipitation that developed locally in the KP, precipitation signals arose south of 30°N in the 12th window. These characteristics appeared in both periods, but the magnitude and disappearance of the precipitation signals were different between P1 and P2.

Compared to the first EEOF mode in P1, a broader and stronger precipitation core appeared in the Satsunan Islands and Okinawa, and a weaker precipitation signal appeared in the KP in the first window in P2. Subsequently, the spatio-temporal evolution shifted northward in the fifth window and rapidly disappeared in the eighth window. The precipitation signal that developed south of 30°N shifted to the earlier two windows compared to that of P1. In the 13th and 14th windows, the local precipitation signal located at the KP became weaker compared to that of P1.

This transition from P1 to P2 demonstrated that throughout the recent two decades, the precipitation core that developed in the early boreal summer (the first window to the fifth window) became stronger with time, whereas the precipitation core generally weakened in the middle period (after the sixth window). Thus, the climatological sub-seasonal mode of precipitation associated with heavy rainfall in the EA region has recently become stronger and shorter. The difference between the maximum and minimum rainfall in P2 compared to P1 is inconsistent and shows different changes depending on the window. In addition, the pattern correlations in 1–3 windows are very similar, but the difference in intensity during P2 is characterized by a larger difference. However, during 9–14 windows, the intensity difference of P1 rather increases, the pattern correlation drops to 0.44, and the sub-seasonal mode shows various changes depending on the window, so it is difficult to explain only the PC time series (Fig. 7).

4 Summary and Discussion

This study analyzed the trend and variability of the summer mean and extreme precipitation from 1973 to 2022. Until the mid-1990s, the ERA5 was similar to the observations.

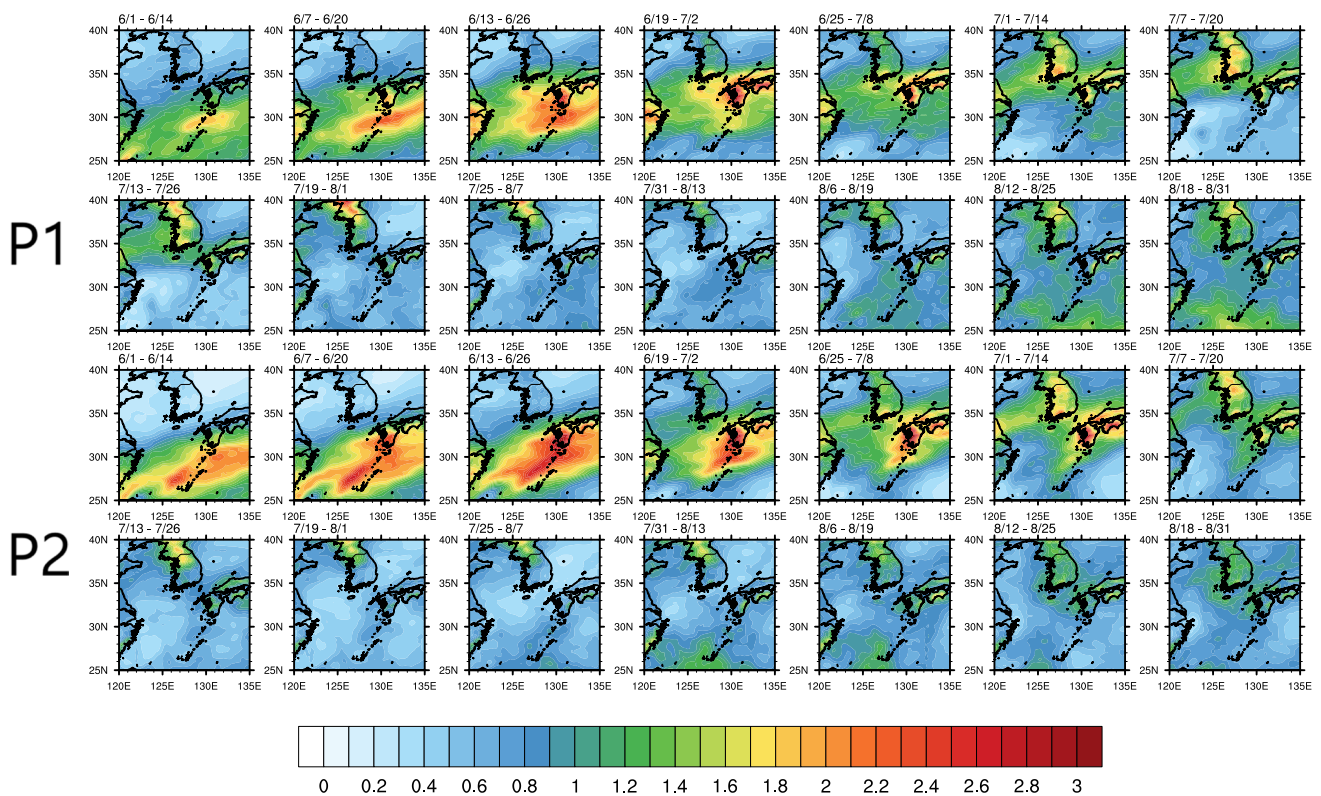


Fig. 6 The temporal evolution of the spatial distribution of the first EEOF mode of daily precipitation from June to August for P1 (1973–1992) and P2 (2003–2022)

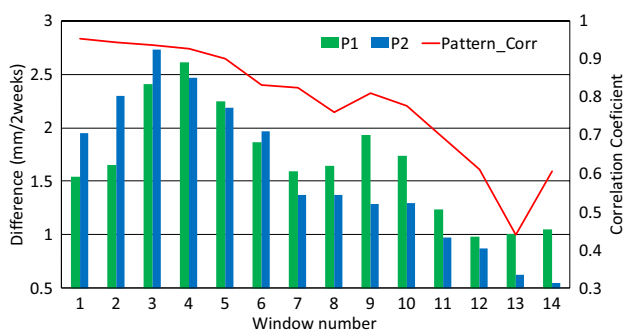


Fig. 7 The pattern correlation (red line) between P1 and P2 and the difference between maximum location and minimum location (bar) as each window

However, since the late 1990s, precipitation from the reanalysis dataset has tended to be underestimated, particularly at the peak of precipitation. This implied that torrential rainfall became more localized, and it was difficult to capture extreme events on a sub-grid scale solely using the reanalysis dataset. Therefore, observational data were invaluable for studying extreme rainfall events. Generally, precipitation indices, in terms of intensity and frequency, showed an increasing trend from 1973 to 2022. One noteworthy

result was a significant increase in the hourly-maximum precipitation, whereas the mean precipitation presented a slight increase. In terms of frequency, the number of R99p days became significantly more frequent. Regarding spatial distribution, summer precipitation exhibited greater spatial variability across South Korea. In general, it was illustrated that an increasing trend of mean and extreme precipitation occurred in the northern part of the central region and some southern coastal regions of the KP. Additionally, RX1H, R95p, and R95pF increased in some coastal and inland areas.

Changes in mean and extreme precipitation were identified in two periods; P1 and P2. All rainfall indices were higher during the latter period than during the former period. Four extreme indices (R95p, R99p, R95pF, and R99pF) were concentrated in July, August, and June. In P2, this trend strengthened, showing reduced intensity in June (except for R99pF) and strengthening in July and August. Owing to the larger increase in July, extreme precipitation appeared to decrease in August. At the sub-seasonal scale, we implemented the EEOF analysis to investigate the temporal evolution of the sub-seasonal mode. The precipitation core occurred at 30°N from early to mid-June. Over time, it evolved and shifted to the KP. This core weakened from mid-July to early August, but another precipitation signal

reappeared near 30°N by mid-August. Although these features occurred in both P1 and P2, there were differences in the intensity and disappearance of the rainfall signals. During P2, this characteristic manifested with a stronger intensity of the major rainband in the early summer and the core became weakened after mid-July. These results indicated that the climatological sub-seasonal mode of summer precipitation in the EA region has become intensified and shorter in recent decades.

In terms of long-term variations, we found that changes in the mean temperature and PRCPTOT occurred at different times. The higher phase of the mean temperature, above the mean value, was reached in the mid-2000s and stabilized in 2010. However, PRCPTOT achieved a higher phase between the mid-1990s and 2010. Similarly, additional extreme precipitation indices, such as RX1H, R95p, and R20mm, showed similar characteristics to PRCPTOT. The dry day had a negative correlation with PRCPTOT. In other words, increases in the intensity and frequency of extreme rainfall had a major impact on the total quantity of summer precipitation in recent years. Moreover, PRCPTOT, RX1H, and R95p were elevated in urbanized regions.

Our results provided a foundation for understanding the mean and extreme precipitation in South Korea in terms of trends, spatio-temporal variability, and long-term variation. First, we emphasized the importance of observational data in the study of heavy rainfall. Second, extreme rainfall had increased more than mean precipitation during the last five decades. In particular, hourly-maximum precipitation increased significantly. Third, extreme precipitation played a greater role in summer precipitation, and several extreme precipitation indices appeared higher in urbanized areas. Finally, the intensification of the rainband occurred sooner over the recent two decades. The results of this study suggested that extreme precipitation events would occur more frequently and with greater intensity in the future. In the event of rapid and extreme rainfall, we should be cautious and well-prepared.

Supplementary Information The online version contains supplementary material available at <https://doi.org/10.1007/s13143-023-00323-7>.

Acknowledgements This work was supported by a 2021-Year Culture Award Grant of Busan City. We acknowledge Haeun Jeon and Woojin Jung for collecting data.

Data Availability The ASOS data presented in this study are provided by Korea Meteorological Administration (KMA). The ERA5 dataset can be found at “<https://www.ecmwf.int/en/forecasts/datasets/reanalysis-datasets/era5>”.

Declarations

Conflict of Interest The authors declare that they have no conflict of interest.

References

- Alexander, L.V., Zhang, X., Peterson, T. C., Caesar, J., Gleason, B., Klein Tank, A. M. G., Haylock, M., Collins, D., Trewin, B., Rahimzadeh, F., Tagipour, A., Rupa Kumar, K., Revadekar, J., Griffiths, G., Vincent, L., Stephenson, D. B., Burn, J., Aguilar, E., Brunet, M., ... Vazquez-Aguirre, J. L.: Global observed changes in daily climate extremes of temperature and precipitation. *J. Geophys. Res. Atmos.* **111**(5) (2006). <https://doi.org/10.1029/2005JD006290>
- Allan, R.P., Soden, B.J.: Atmospheric Warming and the Amplification of Precipitation Extremes. *Science* **321**(5895), 1481–1484 (2008). <https://doi.org/10.1126/science.1107142>
- Allen, M.R., Ingram, W.J.: Constraints on future changes in climate and the hydrologic cycle. *Nature* (2002). www.nature.com/nature
- Amante, C., Eakins, B.W.: NOAA Technical Memorandum NESDIS NGDC-24 ETOPO1 1 ARC-minute global relief model: Procedures, data sources and analysis. (2009)
- An, S.-L., Ha, K.-J., Seo, K.-H., Yeh, S.-W., Min, S.-K., Ho, C.-H., (2011). A Review of Recent Climate Trends and Causes over the Korean Peninsula. *J. Clim. Change Res.* **2**(4), 237–251. www.dbpia.co.kr
- Azam, M., Maeng, S. J., Kim, H. S., Lee, S. W., Lee, J. E. (2018). Spatial and temporal trend analysis of precipitation and drought in South Korea. *Water (Switzerland)* **10**(6). <https://doi.org/10.3390/w10060765>
- Bae, G., Yeung, J.: Record rainfall kills at least 9 in Seoul as water floods buildings, submerges cars. *CNN* (2022)
- Baek, H.J., Kim, M.K., Kwon, W.T.: Observed short- and long-term changes in summer precipitation over South Korea and their links to large-scale circulation anomalies. *Int. J. Climatol.* **37**(2), 972–986 (2017). <https://doi.org/10.1002/joc.4753>
- Borodina, A., Fischer, E.M., Knutti, R.: Models are likely to underestimate increase in heavy rainfall in the extratropical regions with high rainfall intensity. *Geophys. Res. Lett.* **44**(14), 7401–7409 (2017). <https://doi.org/10.1002/2017GL074530>
- Chen, J.-M., Harr, P.A.: Interpretation of Extended Empirical Orthogonal Function (EEOF) Analysis. *Mon. Weather Rev.* **121**, 2631–2636 (1993)
- Chou, C., Chen, C.A., Tan, P.H., Chen, K.T.: Mechanisms for global warming impacts on precipitation frequency and intensity. *J. Clim.* **25**(9), 3291–3306 (2012). <https://doi.org/10.1175/JCLI-D-11-00239.1>
- Craig, R.K.: “Stationarity is dead”—Long live transformation: Five principles for climate change adaptation law. A. An Introduction to climate change adaptation and its differences from mitigation. B. The need to turn legal attention to climate change adaptation. *Harvard Environ. Law Rev.* **34**(1), 9–73 (2010)
- Dave, R., Subramanian, S.S., Bhatia, U.: Extreme precipitation induced concurrent events trigger prolonged disruptions in regional road networks. *Environ. Res. Lett.* **16**(10) (2021). <https://doi.org/10.1088/1748-9326/ac2d67>
- Ha, K.J., Ha, E.H., Yoon, C.S., Jeon, E.H.: Temperature trends and extreme climate since 1909 at big four cities of Korea [in Korean]. *J. Korean Meteorol. Soc.* **40**(1), 1–16 (2004)
- Ha, K.-J., Moon, S., Timmermann, A., Kim, D.: Future Changes of Summer Monsoon Characteristics and Evaporative Demand Over Asia in CMIP6 Simulations. *Geophys. Res. Lett.* **47**(8) (2020a). <https://doi.org/10.1029/2020GL087492>
- Ha, K.-J., Yeo, J.H., Seo, Y.W., Chung, E.S., Moon, J.Y., Feng, X., Lee, Y.W., Ho, C.H.: What caused the extraordinarily hot 2018 summer in Korea? *J. Meteorol. Soc. Jpn* **98**(1), 153–167 (2020b). <https://doi.org/10.2151/jmsj.2020-009>
- Ha, K.-J., Oh, H.: Multifaceted Intraseasonal Modes in the East Asian-Western North Pacific Summer Monsoon Climate. In: *The Multi-scale Global Monsoon System: Vol. Volume 11* (pp. 37–47). World Scientific (2019). https://doi.org/10.1142/9789811216602_0004

- Ha, K.-J., Yun, K.-S., Jhun, J.-G., Li, J.: Circulation changes associated with the interdecadal shift of Korean August rainfall around late 1960s. *J. Geophys. Res. Atmos.* **114**(D4) (2009). <https://doi.org/10.1029/2008JD011287>
- Held, I.M., Soden, B.J.: Robust Responses of the Hydrological Cycle to Global Warming. *J. Clim.* **19**(21), 5686–5699 (2006)
- Hersbach, H., Bell, B., Berrisford, P., Hirahara, S., Horányi, A., Muñoz-Sabater, J., Nicolas, J., Peubey, C., Radu, R., Schepers, D., Simmons, A., Soci, C., Abdalla, S., Abellan, X., Balsamo, G., Bechtold, P., Biavati, G., Bidlot, J., Bonavita, M., ... Thépaut, J. N.: The ERA5 global reanalysis. *Q. J. R. Meteorol. Soc.* **146**(730), 1999–2049 (2020). <https://doi.org/10.1002/qj.3803>
- Ho, C.H., Lee, J.Y., Ahn, M.H., Lee, H.S.: A sudden change in summer rainfall characteristics in Korea during the late 1970s. *Int. J. Climatol.* **23**(1), 117–128 (2003). <https://doi.org/10.1002/joc.864>
- IPCC: Climate Change 2022: Impacts, Adaptation, and Vulnerability. Contribution of Working Group II to the Sixth Assessment Report of the Intergovernmental Panel on Climate Change. In: Pörtner, H.-O., Roberts, D.C., Tignor, M., Poloczanska, E.S., Minterbeck, K., Alegria, A., Craig, M., Langsdorf, S., Löschke, S., Möller, V., Okem, A., Rama, B. (eds.). 3056 pp. Cambridge University Press, Cambridge, UK and New York, NY, USA (2022). <https://doi.org/10.1017/9781009325844>
- Hu, W., Chen, L., Shen, J., Yao, J., He, Q., Chen, J.: Changes in Extreme Precipitation on the Tibetan Plateau and Its Surroundings: Trends, Patterns, and Relationship with Ocean Oscillation Factors. *Water* **14**(16) (2022). <https://doi.org/10.3390/w14162509>
- Jeong, Y., Nam, S., Kwon, J.-I., Uppara, U., Jo, Y.-H.: Surface Warming Slowdown With Continued Subsurface Warming in the East Sea (Japan Sea) Over Recent Decades (2000–2014). *Front. Mar. Sci.* **9** (2022). <https://doi.org/10.3389/fmars.2022.825368>
- Jia, Z., Zheng, Z., Feng, G., Tong, M.: The Intraseasonal Variations of the Leading Mode of Summer Precipitation Anomalies in Meiyu Area of East Asia. *Atmosphere* **13**(2) (2022). <https://doi.org/10.3390/atmos13020217>
- Jung, H.S., Choi, Y., Oh, J.H., Lim, G.H.: Recent trends in temperature and precipitation over South Korea. *Int. J. Climatol.* **22**(11), 1327–1337 (2002). <https://doi.org/10.1002/joc.797>
- Jung, I.W., Bae, D.H., Kim, G.: Recent trends of mean and extreme precipitation in Korea. *Int. J. Climatol.* **31**(3), 359–370 (2011). <https://doi.org/10.1002/joc.2068>
- Kharin, V.V., Zwiers, F.W., Zhang, X., Hegerl, G.C.: Changes in temperature and precipitation extremes in the IPCC ensemble of global coupled model simulations. *J. Clim.* **20**(8), 1419–1444 (2007). <https://doi.org/10.1175/JCLI4066.1>
- Kim, H., Lee, J.-H., Park, H.-J., Heo, J.-H.: Assessment of temporal probability for rainfall-induced landslides based on nonstationary extreme value analysis. *Eng. Geol.* **294** (2021). <https://doi.org/10.1016/j.enggeo.2021.106372>
- Kim, J., Choi, J., Choi, C., Park, S.: Impacts of changes in climate and land use/land cover under IPCC RCP scenarios on streamflow in the Hoeya River Basin, Korea. *Sci. Total Environ.* **452–453**, 181–195 (2013). <https://doi.org/10.1016/j.scitotenv.2013.02.005>
- Kim, J.H., Wu, C.C., Sui, C.H., Ho, C.H.: Tropical cyclone contribution to interdecadal change in summer rainfall over South China in the early 1990s. *Terr. Atmos. Ocean. Sci.* **23**(1), 49–58 (2012). [https://doi.org/10.3319/TAO.2011.08.26.01\(A\)](https://doi.org/10.3319/TAO.2011.08.26.01(A))
- Kim, K.Y., Kitoh, A., Ha, K.J.: The SST-forced predictability of the sub-seasonal mode over East Asia with an atmospheric general circulation model. *Int. J. Climatol.* **28**(12), 1599–1606 (2008). <https://doi.org/10.1002/joc.1655>
- Kim, S., Ha, K.-J.: Interannual and decadal covariabilities in East Asian and Western North Pacific summer rainfall for 1979–2016. *Clim. Dyn.* **56**(3), 1017–1033 (2021). <https://doi.org/10.1007/s00382-020-05517-7>
- Kim, T., Shin, J.Y., Kim, S., Heo, J.H.: Identification of relationships between climate indices and long-term precipitation in South Korea using ensemble empirical mode decomposition. *J. Hydrol.* **557**, 726–739 (2018)
- KMA.: Abnormal Climate Report 2020 (in Korean). KMA, pp., 212 (2021). <http://www.climate.go.kr/home/bbs/view.php?code=93&bname=abnormal&vcode=6494>
- Kripalani, R., Ha, K.J., Ho, C.H., Oh, J.H., Preethi, B., Mujumdar, M., Prabhu, A.: Erratic Asian Monsoon 2022: COVID-19 lockdown initiates possible cause for these episodes? *Clim. Dyn.* **59**, 1339–1352 (2022). <https://doi.org/10.1007/s00382-021-06042-x>
- Lee, J.-Y., Kwon, M., Yun, K.-S., Min, S.-K., Park, I.-H., Ham, Y.-G., Jin, E.K., Kim, J.-H., Seo, K.-H., Kim, W., Yim, S.-Y., Yoon, J.-H.: The long-term variability of Changma in the East Asian summer monsoon system: A review and revisit. *Asia-Pac. J. Atmos. Sci.* **53**(2), 257–272 (2017). <https://doi.org/10.1007/s13143-017-0032-5>
- Lee, M.H., Ho, C.H., Kim, J., Song, C.K.: Assessment of the changes in extreme vulnerability over East Asia due to global warming. *Clim. Change* **113**(2), 301–321 (2012). <https://doi.org/10.1007/s10584-011-0345-9>
- Meyer, J., Neuper, M., Mathias, L., Zehe, E., Pfister, L.: More frequent flash flood events and extreme precipitation favouring atmospheric conditions in temperate regions of Europe. *Hydrol. Earth Syst. Sci.* (2021). <https://doi.org/10.5194/hess-2021-628>
- Min, S.K., Son, S.W., Seo, K.H., Kug, J.S., An, S. il, Choi, Y.S., Jeong, J.H., Kim, B.M., Kim, J.W., Kim, Y.H., Lee, J.Y., Lee, M.I.: Changes in weather and climate extremes over Korea and possible causes: A review. *Asia-Pac. J. Atmos. Sci.* **51**(2), 103–121 (2015). Korean Meteorological Society. <https://doi.org/10.1007/s13143-015-0066-5>
- Min, S.K., Zhang, X., Zwiers, F.W., Hegerl, G.C.: Human contribution to more-intense precipitation extremes. *Nature* **470**(7334), 378–381 (2011). <https://doi.org/10.1038/nature09763>
- Moberg, A., Jones, P.D., Lister, D., Walthers, A., Brunet, M., Jacobeit, J., Alexander, L.V., Della-Marta, P.M., Luterbacher, J., Yiou, P., Chen, D., Tank, A. M.G.K., Saladié, O., Sigró, J., Aguilar, E., Alexandersson, H., Almarza, C., Auer, I., Barriendos, M., ... Xoplaki, E.: Indices for daily temperature and precipitation extremes in Europe analyzed for the period 1901–2000. *J. Geophys. Res. Atmos.* **111**(D22) (2006). <https://doi.org/10.1029/2006JD007103>
- Moon, M., Ha, K.-J.: Abnormal Activities of Tropical Cyclones in 2019 Over the Korean Peninsula. *Geophys. Res. Lett.* **48**(7) (2021). <https://doi.org/10.1029/2020GL090784>
- Ning, G., Luo, M., Zhang, Q., Wang, S., Liu, Z., Yang, Y., Wu, S., Zeng, Z.: Understanding the Mechanisms of Summer Extreme Precipitation Events in Xinjiang of Arid Northwest China. *J. Geophys. Res. Atmos.* **126**(15) (2021). <https://doi.org/10.1029/2020JD034111>
- O’Gorman, P.A., Schneider, T.: The physical basis for increases in precipitation extremes in simulations of 21st-century climate change. *Proc. Natl. Acad. Sci. U.S.A.* **106**(35), 14773–14777 (2009). <https://doi.org/10.1073/pnas.0907610106>
- Oh, H., Ha, K.-J., Timmermann, A.: Disentangling impacts of dynamic and thermodynamic components on late summer rainfall anomalies in East Asia. *J. Geophys. Res. Atmos.* **123** (2018). <https://doi.org/10.1029/2018JD028652>
- Park, B.J., Kim, Y.H., Min, S.K., Kim, M.K., Choi, Y., Boo, K.O., Shim, S.: Long-Term Warming Trends in Korea and Contribution of Urbanization: An Updated Assessment. *J. Geophys. Res. Atmos.* **122**(20), 10637–10654 (2017). <https://doi.org/10.1002/2017JD027167>
- Park, C., Son, S.-W., Kim, H., Ham, Y.-G., Kim, J., Cha, D.-H., Chang, E.-C., Lee, G., Kug, J.-S., Lee, W.-S., Lee, Y.-Y., Lee, H.C., Lim, B.: Record-Breaking Summer Rainfall in South Korea in 2020: Synoptic Characteristics and the Role of Large-Scale Circulations. *Mon. Weather Rev.* **149**, 3085–3100 (2021). <https://doi.org/10.1175/MWR-D>

- Park, H.L., Seo, K.H., Son, J.H.: Development of a dynamics-based statistical prediction model for the Changma onset. *J. Clim.* **28**(17), 6647–6666 (2015). <https://doi.org/10.1175/JCLI-D-14-00502.1>
- Pei, L., Xia, J., Yan, Z., Yang, H.: Assessment of the Pacific decadal oscillation's contribution to the occurrence of local torrential rainfall in north China. *Clim. Change* **144**(3), 391–403 (2017). <https://doi.org/10.1007/s10584-016-1610-8>
- Preethi, B., Mujumdar, M., Kripalani, R.H., Prabhu, A., Krishnan, R.: Recent trends and teleconnections among South and East Asian summer monsoons in a warming environment. *Clim. Dyn.* **48**, 2489–2505 (2017). <https://doi.org/10.1007/s00382-016-3218-0>
- Ren, Q., Liu, F., Wang, B., Yang, S., Wang, H., Dong, W.: Origins of the Intraseasonal Variability of East Asian Summer Precipitation. *Geophys. Res. Lett.* **49**(4) (2022). <https://doi.org/10.1029/2021GL096574>
- Ryan, C., Curley, M., Walsh, S., Murphy, C.: Long-term trends in extreme precipitation indices in Ireland. *Int. J. Climatol.* **42**(7), 4040–4061 (2022). <https://doi.org/10.1002/joc.7475>
- Seo, K.-H., Son, J.-H., Lee, J.-Y.: A New Look at Changma. *Atmosphere* **21**, 109–121 (2011)
- Seo, Y. W., Ha, K.-J., Park, T. W.: Feedback attribution to dry heatwaves over East Asia. *Environ. Res. Lett.* **16**(6) (2021). <https://doi.org/10.1088/1748-9326/abf18f>
- Trenberth, K.E., Dai, A., Rasmussen, R.M., Parsons, D.B.: The changing character of precipitation. *Bull. Am. Meteor. Soc.* **84**(9), 1205–1218 (2003)
- Wang, B., Biasutti, M., Byrne, M.P., Castro, C., Chang, C.-P., Cook, K., Fu, R., Grimm, A.M., Ha, K.-J., Hendon, H., Kitoh, A., Krishnan, R., Lee, J.-Y., Li, J., Liu, J., Moise, A., Pascale, S., Roxy, M.K., Seth, A., ... Zhou, T.: Monsoons Climate Change Assessment. *Bull. Am. Meteorol. Soc.* **102**(1), E1–E19 (2021). <https://doi.org/10.1175/BAMS-D-19-0335.1>
- Wu, Z., Huang, N. E.: A study of the characteristics of white noise using the empirical mode decomposition method. *Proc. R. Soc. Lond. A Math. Phys. Eng. Sci.* **460**(2046), 1597–1611 (2004). <https://doi.org/10.1098/rspa.2003.1221>
- Wu, Z., Huang, N.E.: Ensemble empirical mode decomposition: a noise-assisted data analysis method. *Adv. Adapt. Data Anal.* **01**(01), 1–41 (2009). <https://doi.org/10.1142/S1793536909000047>
- Yao, C., Yang, S., Qian, W., Lin, Z., Wen, M.: Regional summer precipitation events in Asia and their changes in the past decades. *J. Geophys. Res. Atmos.* **113**(17) (2008). <https://doi.org/10.1029/2007JD009603>
- Yun, J., Ha, K.-J., Jo, Y.-H.: Interdecadal changes in winter surface air temperature over East Asia and their possible causes. *Clim. Dyn.* **51**(4), 1375–1390 (2018). <https://doi.org/10.1007/s00382-017-3960-y>

Publisher's Note Springer Nature remains neutral with regard to jurisdictional claims in published maps and institutional affiliations.

Springer Nature or its licensor (e.g. a society or other partner) holds exclusive rights to this article under a publishing agreement with the author(s) or other rightsholder(s); author self-archiving of the accepted manuscript version of this article is solely governed by the terms of such publishing agreement and applicable law.